



Deposited via The University of Sheffield.

White Rose Research Online URL for this paper:

<https://eprints.whiterose.ac.uk/id/eprint/96977/>

Version: Accepted Version

Article:

Gasson, E., DeConto, R.M., Pollard, D. et al. (2016) Dynamic Antarctic ice sheet during the early to mid-Miocene. *Proceedings of the National Academy of Sciences*, 113 (13).

<https://doi.org/10.1073/pnas.1516130113>

Reuse

Items deposited in White Rose Research Online are protected by copyright, with all rights reserved unless indicated otherwise. They may be downloaded and/or printed for private study, or other acts as permitted by national copyright laws. The publisher or other rights holders may allow further reproduction and re-use of the full text version. This is indicated by the licence information on the White Rose Research Online record for the item.

Takedown

If you consider content in White Rose Research Online to be in breach of UK law, please notify us by emailing eprints@whiterose.ac.uk including the URL of the record and the reason for the withdrawal request.

A dynamic Antarctic Ice Sheet during the early to middle Miocene

Edward Gasson¹, Robert DeConto¹, David Pollard², Richard Levy³

¹Climate System Research Center, University of Massachusetts, Amherst, MA, 01003, USA ²Earth and Environmental Systems Institute, Pennsylvania State University, State College, PA, 16802, USA ³GNS Science, Avalon, Lower Hutt 5011, New Zealand

Submitted to Proceedings of the National Academy of Sciences of the United States of America

Geological data indicate that there were major variations in Antarctic ice sheet volume and extent during the early to middle Miocene. Simulating such large-scale changes is problematic because of a strong hysteresis effect, which results in stable ice sheets once they have reached continental size. A relatively narrow range of atmospheric CO₂ concentrations indicated by proxy records exacerbates this problem. Here we are able to simulate large-scale variability of the Miocene Antarctic ice sheet for the first time due to three developments in our modeling approach: 1. We use a new climate-ice sheet coupling method using a high-resolution atmospheric component, to account for ice sheet-climate feedbacks 2. The ice sheet model includes recently proposed mechanisms for retreat into deep subglacial basins caused by ice-cliff failure and ice-shelf hydrofracture 3. We account for changes in the oxygen isotopic composition of the ice sheet by using isotope enabled climate and ice sheet models. We compare our modeling results with new ice-proximal records emerging from a sedimentological drill core from the Ross Sea (Andrill-2A) that is presented in a companion paper. The variability in Antarctic ice volume we simulate is equivalent to a seawater oxygen isotope signal of 0.52–0.66 ‰, or a sea level equivalent change of 30–36 m, for a range of atmospheric CO₂ between 280–500 ppm and a changing astronomical configuration. This result represents a substantial advance in resolving the long-standing model-data conflict of Miocene Antarctic ice sheet and sea level variability.

Miocene | Antarctic ice sheet | oxygen isotopes | sea level

Both direct and indirect evidence indicates that the Antarctic ice sheet exhibited major variation in volume and extent during the early to middle Miocene (23–14 million years ago, Ma). Indirect evidence for a change in Antarctic ice volume comes from δ¹⁸O records of benthic foraminifera [1–5] and sea-level indicators [6–8]. Although the benthic δ¹⁸O record contains a mixed signal of ice volume and ocean temperature, attempts to isolate the ice volume component show variability equivalent to the loss of between 30% [2,3] and 80% [4,5,9] of the modern Antarctic ice sheet. A similar magnitude of variability is indicated by sea level estimates [6–8]. This may represent periods of ice advance with volumes greater than modern and periods of retreat with significant (but not complete) loss of ice.

Direct evidence of the Miocene Antarctic environment can be found in ocean sediments drilled at sites proximal to the ice sheet, such as the Andrill 2A (AND-2A) drill core in the southern McMurdo Sound region of the Ross Sea (see companion paper). These records show warmer conditions in the Ross Sea region during the middle Miocene climatic optimum, with summer atmospheric temperatures of ~10 °C and annual mean sea-surface temperatures between 0–11.5 °C [10,11]. During these warmer intervals the ice sheet margins retreated inland [12,13] and tundra vegetation grew on ice-free terrain [10,14]. During cold intervals the ice sheet expanded, with grounded ice extending into the Ross Sea basins, beyond the AND-2A drill site [12].

Importantly, proxy reconstructions of atmospheric CO₂ concentrations through this interval imply that this variability occurred in a relatively narrow range from close to, or slightly below,

preindustrial levels [15–18] to maximum concentrations of only ~500 ppm [15,16,18,19].

Simulating such large-scale variability of the Antarctic ice sheet with this narrow range of atmospheric CO₂ has proved problematic [20,21]. This is due to a strong hysteresis, which limits retreat from a fully glaciated state until surface temperatures have increased by 15–20 °C [22] or atmospheric CO₂ has reached 1000–2500 ppm [20, 23]; see also *Supporting Information*. This hysteresis occurs because of surface elevation-mass balance feedback as a result of the atmospheric lapse rate [24], and is further strengthened by albedo feedback [20] and possibly the cooling effect of the ice sheet on the surrounding Southern Ocean [56].

Recent efforts at resolving the Antarctic hysteresis problem have focused on the marine-based regions of the ice sheets [23,25]. This work has been stimulated in part by evidence for major retreat into the Wilkes Subglacial Basin during warmer intervals of the middle Pliocene [26] and the need to explain the, albeit uncertain, 20 ±10 m middle Pliocene sea level highstand [27,28]. Additionally, the marine-based ice sheet regions are thought to be more sensitive to climate changes than the terrestrial-based regions because of instability mechanisms that act only on marine-based ice, particularly where the ice sits on reverse-sloped beds [23,29,30]. However, only a third of the modern Antarctic ice sheet is marine-based [31], which suggests that the variability during the Miocene also included changes in terrestrial ice sheet extent.

Evidence of grounded ice in the western Ross Sea during the Miocene provides another modeling challenge. Simulating a large, grounded West Antarctic ice sheet typically requires Last Glacial Maximum-like conditions, with low atmospheric CO₂ of ~180 ppm, cold ocean temperatures, and lowered sea level

Significance

Atmospheric concentrations of carbon dioxide are projected to exceed 500 ppm in the coming decades. It is likely that the last time such levels of atmospheric CO₂ were reached was during the Miocene, for which there is geologic data for large-scale advance and retreat of the Antarctic ice sheet. This is something that ice sheet models have struggled to replicate because of a strong hysteresis effect. Here a number of developments in our modeling approach mean that we are able to simulate large-scale variability of the Miocene Antarctic ice sheet for the first time. Our results are also consistent with a recently recovered sedimentological record from the Ross Sea presented in a companion paper.

Reserved for Publication Footnotes

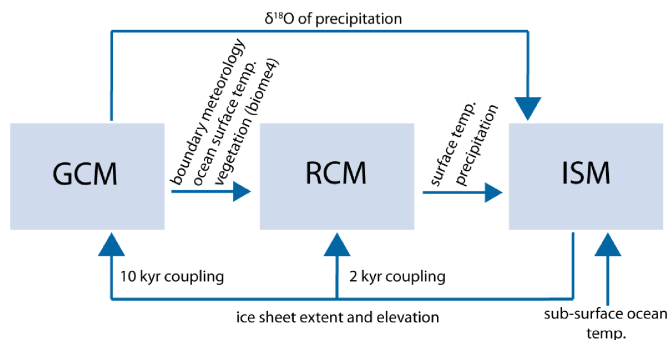


Fig. 1. Schematic of model coupling procedure, showing variables passed between models and timestep of couplings.

allowing grounding lines to advance seaward to the continental shelf break. Such low atmospheric CO₂ is below the glacial threshold for major Northern Hemisphere glaciation [33], but there is limited evidence for such major Northern Hemisphere glaciation during the Miocene [16], making the conditions for simulating grounded ice in the western Ross Sea problematic.

Periods with grounded ice are identified in the AND-2A record as disconformities, when the advancing ice sheet eroded material at the site. Four such episodes occurred during the early to middle Miocene and correlate with benthic δ¹⁸O and sea level records supporting increased ice volume. Additionally, these ice advances correlate with lows in atmospheric CO₂ and decreasing bottom water temperatures. Regional seismic data provide supporting evidence that the West Antarctic ice sheet was periodically grounded towards the Ross Sea shelf edge during the middle Miocene [51].

In the companion paper different environmental motifs are identified from the AND-2A sediment core, here we attempt to simulate these different environmental motifs. In addition we attempt to simulate the magnitude of ice volume variability that is suggested from indirect proxy evidence whilst using appropriate Miocene boundary conditions.

Results

Changes in ice sheet extent can affect the surface climate, because of changes in elevation, surface albedo and large-scale circulation changes [50,67]. Various methods for accounting for these feedbacks are discussed in [50] and briefly in the *Supporting Information*. Here, to account for ice sheet-climate feedbacks caused by albedo changes, changes in vegetation, and atmospheric circulation changes, we use a high resolution climate forcing from an asynchronously coupled Regional Climate Model (RCM) embedded in a GCM (Figure 1). The GCM is oxygen isotope enabled and includes a vegetation model to account for vegetation-albedo feedbacks. Simulations are also performed without climate feedbacks, to determine the impact of including these feedbacks on the results (see Methods and Materials).

Miocene colder interval simulations. End-member climate-ice sheet simulations were performed for Miocene ‘colder’ and ‘warmer’ climate intervals. The colder climate forcing has atmospheric CO₂ concentrations of 280 ppm and an astronomical configuration favorable for Antarctic glaciation (low obliquity, high eccentricity, perihelion during boreal summer).

The bedrock topography is an important model boundary condition that affects ice sheet stability because of marine instabilities and ice-cliff failure [23,49]. However, Antarctic bedrock topography is poorly constrained for the Miocene. The Antarctic bedrock topography has changed through time, due in part to tectonics, dynamic topography, continental shelf progradation, and glacial erosion following continental glaciation across the Eocene-Oligocene transition [34,61]. The amount of material

removed from the continent can be loosely constrained by volumes of Oligocene and younger sediments deposited offshore of the continent; Wilson *et al.* [34] used this as a basis for their topographic reconstruction for the Eocene-Oligocene transition.

As, to our knowledge, no reconstructed topography for the Miocene currently exists, we created a middle Miocene topography by scaling between the earlier Eocene-Oligocene topography [34] and the isostatically rebounded (ice-free) modern topography [41], assuming constant rates of landscape evolution from 34 Ma to today. An alternative view is that the Antarctic ice sheet had stabilized by 14 Ma [35], implying that the majority of glacial erosion had already occurred by this time [64] and that the bedrock topography may have been similar to modern after the middle Miocene. Experiments were performed for two bedrock topography scenarios, one is the modern bedrock topography (*Scenario A*) and the second is an approximation of the Miocene bedrock topography (*Scenario B*). The differences in bathymetry are shown in Fig. 2, with topographic maps and sensitivity tests for a range of other topographies in *Supporting Information*.

For the colder climate simulations, the different bedrock topographies have a large impact on the resulting ice sheet (see Fig. 2 C and D and Table 1). Total ice volumes vary between 26.7–35.5 × 10⁶ km³ for *Scenario A* and *B*, respectively, or 58–78 m sea level equivalent (msl). The shallower bathymetry in the West Antarctic for *Scenario B* allows a large terrestrial ice sheet to form (15 msl), which supports the further expansion of the East Antarctic ice sheet. Only *Scenario B* has grounded ice at the site of AND-2A and extending to the continental shelf break. For *Scenario A* there are ice shelves in the Ross Sea and the grounding line is very close to its modern position, several hundred km from the AND-2A site.

Miocene warmer interval simulations. For the warmer climate simulations atmospheric CO₂ concentrations are increased to 500 ppm and an astronomical configuration favorable for Antarctic deglaciation is used (high obliquity, high eccentricity, perihelion during austral summer). Although Miocene atmospheric CO₂ appears poorly constrained if all published estimates and proxy methods are considered, some of these methods and estimates have been subsequently discredited [63]. Additionally, the low temporal resolution of the majority of these records may not fully capture astronomically paced changes in atmospheric CO₂ [18], which may be indicated by high temporal resolution carbon isotope records [62]. Whilst acknowledging these uncertainties, there is a growing consensus that atmospheric CO₂ varied between 280–500 ppm during the Miocene [15,16,18,19]. Because there is at least one estimate of mid-Miocene CO₂ as high as ~840 ppm [36], we perform an additional high CO₂ simulation with atmospheric CO₂ of 840 ppm.

In addition to changes in atmospheric CO₂ concentrations and the astronomical configuration, the warmer climate simulations have 2 °C of imposed ocean-warming relative to modern. This ocean warming is conservatively based on the lower end of reconstructed temperatures at AND-2A in the companion paper. The warmer interval ice sheet simulations were performed starting from a fully glaciated state (from the end of the colder climate simulations) in order to investigate ice sheet hysteresis. Like the colder interval simulations, warmer interval simulations were also performed on two different bedrock topographies. For *Scenario A*, using modern bedrock topography, there is major retreat into the subglacial basins on East Antarctica (Fig. 2E). The Miocene bedrock topography used for *Scenario B* has much shallower marine basins. As a result there is much reduced retreat into the East Antarctic basins for *Scenario B*, with only modest retreat into the Recovery Glacier and the Wilkes Subglacial Basin (Fig. 2F).

The strong sensitivity shown by the ice sheet model to these differences in bedrock topography is mainly a result of two mech-

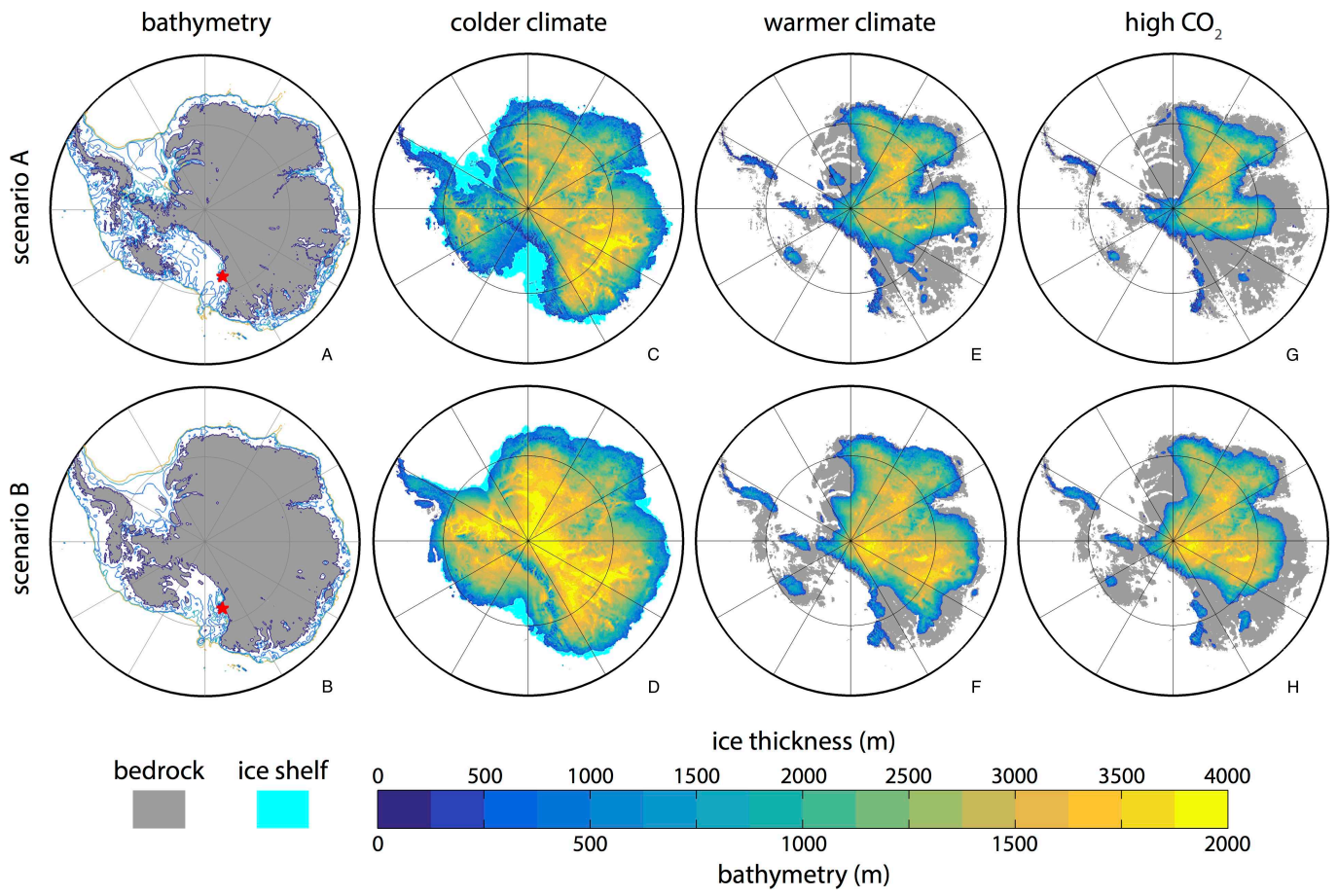


Fig. 2. Ice sheet thickness, in response to different climate forcing. The top row (Scenario A) uses the modern Bedmap2 bedrock topography, the lower row (Scenario B) uses approximate mid Miocene bedrock topography. The differences in bathymetry between these two scenarios are shown, will detailed topographic maps included in *Supporting Information*. Miocene colder interval simulations have atmospheric CO₂ of 280 ppm and an astronomical configuration favorable for Antarctic glaciation (low obliquity, high eccentricity, perihelion during boreal summer). Miocene warmer interval simulations have atmospheric CO₂ of 500 ppm and an astronomical configuration favorable for Antarctic deglaciation (high obliquity, high eccentricity, perihelion during austral summer) and 2 °C of ocean warming. High CO₂ simulations are as the warmer climate simulations but with atmospheric CO₂ raised to 840 ppm. All simulations include climate-ice sheet feedbacks. The red stars mark the location of the AND-2A core site.

Table 1. Ice volume, sea level equivalence and oxygen isotopes. Scenario A uses modern topography, Scenario B uses approximate mid Miocene topography, high eccentricity (0.05) is used for all simulations. Sea levels are calculated for ice above floatation. Peak Sea Surface Temperatures (SST) and peak Land Air Temperatures (LAT) are the mean of the 3 warmest months at the site of, or land proximal to, AND-2A. Cooler climate simulations do not have open-water at site of AND-2A or proximal ice-free land.

| | Scenario A | | | Scenario B | | |
|--|----------------|----------------|----------------------|----------------|----------------|----------------------|
| experiment | colder climate | warmer climate | high CO ₂ | colder climate | warmer climate | high CO ₂ |
| CO ₂ , ppm | 280 | 500 | 840 | 280 | 500 | 840 |
| precession, ° | 90 | 270 | 270 | 90 | 270 | 270 |
| obliquity, ° | 22.5 | 24.5 | 24.5 | 22.5 | 24.5 | 24.5 |
| ice volume, km ³ | 26.7 | 11.5 | 8.8 | 35.5 | 17.2 | 14.1 |
| sea level, m | 57.9 | 28.4 | 21.8 | 78.3 | 42.2 | 34.5 |
| δ ¹⁸ O _{ice} , ‰ | -46.1 | -39.4 | -39.3 | -47.9 | -42.3 | -41.6 |
| δ ¹⁸ O _{sw} , ‰ | 0.82 | 0.3 | 0.23 | 1.14 | 0.48 | 0.38 |
| δ ¹⁸ O _{sw} / 100m | 1.24 | 1.05 | 1.04 | 1.29 | 1.12 | 1.10 |
| peak SST, °C | - | 6.3 | 9.6 | - | 6.0 | 9.6 |
| peak LAT, °C | - | 8.5 | 12.0 | - | 7.5 | 12.4 |

anisms. At the grounding line, ice flow is strongly dependent on ice thickness [30], meaning that run-away retreat can occur if the bed deepens upstream of the grounding line [30,39]. Additionally, the ice sheet model includes a mechanism for the structural

failure of large ice cliffs that are not supported by ice shelves [23]. Vulnerable ice cliffs can form because of the removal of ice shelves in warmer climate simulations as a result of ice shelf hydrofracture. In the model, ice cliff failure can only occur when

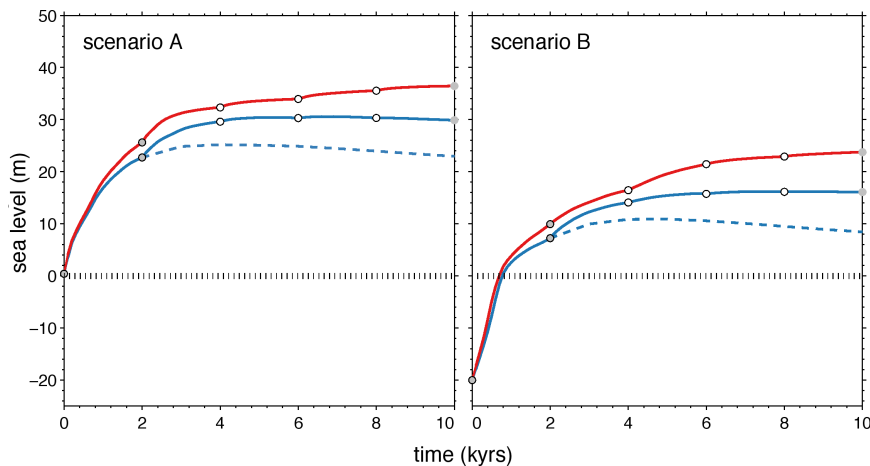


Fig. 3. Timeseries of ice sheet response to warmer climate forcing, shown as sea level equivalent values, for Scenarios A and B. Blue lines are for 500 ppm CO₂ simulation, red lines are for 840 ppm CO₂ simulation. Dashed lines are without climate feedback. Gray dots show GCM simulation and black circles show RCM simulations and subsequent coupling to ice sheet model.

the ice cliff height reaches ~100 m, in water depths of ~800 m [23]. This follows earlier work on the maximum height that ice cliffs can reach before failing structurally [55]. For the Miocene topography with shallower marine basins in East Antarctica, this condition is rarely reached. As the Miocene bedrock topography is highly uncertain we test a variety of different reconstructed bedrock topographies in *Supporting Information*. Although locations of retreat differ between the different topographies, the total ice volume change between the cold and warmer climate simulations is similar (Fig. 3), because of a larger initial West Antarctic ice sheet compensating for reduced retreat of the East Antarctic ice sheet. We also perform tests to determine the importance of ice cliff failure and ice shelf hydrofracture, by repeating the simulations without these mechanisms enabled in the model (see *Supporting Information*).

We next consider how changes in ice sheet $\delta^{18}\text{O}$ ($\delta^{18}\text{O}_{\text{ice}}$) due to changing climate and ice sheet geometry may affect our interpretation of the benthic $\delta^{18}\text{O}$ record [48]. We use an isotope enabled version of the GCM [46] to determine the $\delta^{18}\text{O}$ of precipitation falling over the ice sheet, which is then tracked within the ice sheet to determine the ice sheet's average isotopic composition [58]. For the warmer climate simulations the oxygen isotope composition of precipitation is heavier than for the colder climate simulations (*Supporting Information*). This results in a mean ice sheet $\delta^{18}\text{O}_{\text{ice}}$ of -39 and -42 ‰, for *Scenarios A* and *B*, compared with isotopically lighter values of -46 and -48 ‰ for the colder climate simulations. The difference in seawater $\delta^{18}\text{O}$ ($\delta^{18}\text{O}_{\text{sw}}$) between the colder and warmer climate simulations is 0.52 ‰ for *Scenario A* and 0.66 ‰ for *Scenario B*, because of a combined change in ice volume and mean $\delta^{18}\text{O}_{\text{ice}}$ of the ice sheet. The $\delta^{18}\text{O}_{\text{sw}}$ signal modeled here is greater than if the commonly used factor of 0.01 ‰ per 1 msl were used [48]. Therefore the ice volume change required to explain the oxygen isotope record from benthic foraminifera is lower than previous estimates [4,5,9]. This same reasoning has been used to suggest a reduced ice volume change for the mid-Pliocene [60].

A high CO₂ simulation was also performed, with atmospheric CO₂ of 840 ppm, which is higher than most proxy estimates of atmospheric CO₂ during the Miocene. The high CO₂ simulation may also account for the potential impact of non-CO₂ radiative forcing during past warmer intervals, because of increased methane concentrations or other chemical feedbacks [37], which are not changed from preindustrial in our simulations. For example, the equivalent radiative forcing of 840 ppm CO₂ (5.9 Wm⁻²) can be achieved with atmospheric CO₂ of 720–780 ppm and methane concentrations of 2000–3000 ppb. This elevated

radiative forcing is also necessary to produce the warm high-latitude temperatures shown by proxy reconstructions for the mid-Miocene climatic optimum when using a modern astronomical configuration (*Supporting Information*); similar results were found in an earlier GCM study of the mid-Miocene [38]. However, high-latitude Southern Hemisphere temperatures that are consistent with proxy records can also be achieved with lower CO₂ of 500 ppm if there is a slight increase in the Southern Ocean heat flux [23] and a warm austral astronomical configuration is used.

With this increased range of Miocene CO₂ (280–840 ppm), the total Antarctic ice sheet variability increases to 36 and 44 msl, for *Scenarios A* and *B*, respectively. This variability is equivalent to a change in $\delta^{18}\text{O}_{\text{sw}}$ of between 0.59 and 0.76 ‰. The bedrock topography is again important in determining the magnitude of East Antarctic ice sheet retreat for the high CO₂ experiments (Fig. 2G and H).

The impact of including sheet-climate feedbacks through the asynchronous RCM climate coupling can be seen by comparing simulations without these feedbacks (Fig. 3). Without climate feedback retreat only occurs in the subglacial basins, with retreat of the terrestrial ice sheet restricted by the strong hysteresis. Including climate feedbacks produces some additional retreat at the margins of the terrestrial ice sheet. The asynchronous coupling has a larger effect on ice sheet area compared with volume. This is because increased precipitation in the asynchronous simulations produces a thicker ice sheet interior that cancels some of the increased retreat at the ice sheet margin.

Discussion

We simulate large-scale variability of the early to middle Miocene Antarctic ice sheet of 30–36 msl. Using the output from an isotope enabled GCM and ice sheet model, our simulated $\delta^{18}\text{O}_{\text{sw}}$ signal is 0.52–0.66 ‰. The largest $\delta^{18}\text{O}$ shift during the Miocene was the 0.88 ± 0.04 ‰ increase across the middle Miocene climate transition [47]. This event was also associated with a deep-sea cooling of 1.5 ± 0.5 °C, leaving an ice volume signal of $\delta^{18}\text{O}_{\text{sw}}$ 0.53 ± 0.13 ‰ [5,47]. This magnitude of variability is consistent with our modeled estimates.

We have presented two different scenarios for Antarctic ice sheet variability during the Miocene. One scenario is driven by large-scale retreat into East Antarctic subglacial basins, the second has limited retreat of the East Antarctic ice sheet with variability a result of the expansion of a large terrestrial West Antarctic ice sheet. As both of these scenarios satisfy indirect constraints on ice volume variability during the Miocene indicated by the proxy record [2, 3, 5, 7, 18], we next focus on direct evidence for changes in ice extent as seen in the AND-2A record

(companion paper) to attempt to determine which scenario is the more likely. Data are available from other sectors of Antarctica indicating changes in ice sheet extent during the Miocene, such as the Lambert Glacier region [65,66] and those emerging from a recent Integrated Ocean Drilling Program expedition to Wilkes Land. However, here we focus on the Ross Sea sector, because this is an area that is significantly different between our two modeled scenarios. Future work will focus on other sectors of Antarctica.

The disconformities identified by analysis of the AND-2A drill core in the companion paper indicate that there were intervals during the Miocene with grounded ice in the McMurdo Sound region of the Ross Sea (Environmental Motif I). Only *Scenario B* has grounded ice in this region, because of the shallower topography in the Ross Sea region compared with modern. This requirement for grounded ice at the site of AND-2A may indicate, at least for the Ross Sea region, that *Scenario B* is more appropriate. Our simulations support the interpretation from AND-2A that this glaciation is a result of an expanded continental ice sheet, rather than being a result of local outlet glaciers from the Transantarctic Mountains. A grounded West Antarctic ice sheet extending onto the continental shelf is also consistent with seismic data from the Ross Sea [51].

The transitional environmental motifs interpreted to represent periods with ice shelves (Motif II) or open-water conditions with material delivered by ice-rafting (Motif III) occur in our simulations during the transition from a colder to warmer climate. The final environmental motif, under the warmest climate configuration, assumes open-water conditions in the Ross Sea and ice-free land proximal to the core site (Motif IV). Regardless of the choice of bedrock topography scenario, both of our warmer climate conditions with atmospheric CO₂ of 500 ppm and a warm austral astronomical configuration satisfy these conditions. Simulated sea surface temperatures for these warmer climate simulations are consistent with proxy records [10,11]; the high CO₂ simulations produce temperatures that are greater than indicated by the proxy records (Table 1). The output from the BIOME4 vegetation model embedded within the GCM agrees with geological evidence of Tundra vegetation in proximal areas of exposed ice-free land [10,14].

Even at high atmospheric CO₂ (840 ppm), we do not simulate complete collapse of the East Antarctic ice sheet, with the smallest ice sheet simulated having a volume of 9×10^6 km³ (22 msl). Because this high radiative forcing experiment uses higher greenhouse gas concentrations than required for Antarctic glaciation (using the same climate model) [52], it indicates that a hysteresis does still apply to at least part of the Antarctic ice sheet. It is therefore likely that complete deglaciation of the Antarctic ice sheet would not occur until atmospheric CO₂ has reached the threshold suggested by earlier studies (1000–2500 ppm) [20,22]. This supports the idea that there was a core of stable ice on Antarctica throughout the warm intervals of the early to middle Miocene [18].

Conclusions

The asynchronously coupled climate-ice sheet simulations presented here satisfy the magnitude of Miocene ice sheet variability required by oxygen isotope and sea level records. This magnitude of variability is achieved by a combination of new ice sheet instability mechanisms, an asynchronous GCM-RCM climate forcing and accounting for changes in the mean $\delta^{18}\text{O}$ of the ice sheet. This largely resolves the discrepancy between geological records and ice sheet models that had previously existed. Two different scenarios are presented, due to differences in the bedrock topography, both of which satisfy these indirect constraints. Additional data from other parts of the Antarctic are required to determine which of these two scenarios is more likely in addition to a

detailed synthesis of existing and emerging data. A requirement for grounded ice in the Ross Sea during the middle Miocene is only satisfied by *Scenario B*, which suggests that the Ross Sea continental shelf may have been shallower during the Miocene. The results also support the geological inferences of the AND-2A record indicating that the sedimentological changes at the drill site record large-scale shifts in the ice sheet margin and not just changes in local outlet glaciers. The different scenarios presented here have implications for the suitability of the Miocene as an analog for future Antarctic ice sheet dynamics [57]. If an enlarged and dynamic West Antarctic ice sheet on bedrock bathymetrically higher than today drove Miocene ice volume variability, it is a system that may have less relevance to the future. Alternatively, if retreat was centered on the subglacial basins of the East Antarctic, the East Antarctic ice sheet could have contributed 10s of metres in sea level equivalence with atmospheric CO₂ concentrations similar to that which are projected in the coming decades.

Materials and Methods

The ice sheet model used is a hybrid shallow ice / shallow shelf approximation model, with a parameterization for ice flow across the grounding line based on [30]. Recent developments in the ice sheet model include new mechanisms for ice shelf hydrofracture because of meltwater and precipitation draining into surface crevasses. An additional mechanism is included for the breakup of large ice cliffs that can form in warmer climate simulations following the removal of ice shelves. Failure occurs when ice cliffs are sufficiently large (~100 m), which occurs in subglacial basins with water depths of at least ~800 m [23]. We perform tests without these new mechanisms in *Supporting Information*. Simulations were performed using a resolution of 10×10 km. The ice sheet model is fully documented in [23] and [40] and all parameters are as in [23] unless otherwise stated.

Experiments are performed on two different bedrock topographies in the main paper. For Scenario A the modern Bedmap2 topography is used [31]. For Scenario B an approximate middle Miocene (15 Ma) Antarctic topography was created by scaling between an Eocene-Oligocene (34 Ma) topography [31] and an ice-free, isostatically rebounded version of the modern Bedmap2 topography [41]. This assumes constant landscape evolution through time; we explore ice sheet model sensitivity to a variety of other topographies in the *Supporting Information*.

The climate forcing for the ice sheet model is provided by an asynchronously coupled GCM-RCM. The GCM (GENESIS v3.0 [42,43]) uses a middle Miocene (15 Ma) paleogeography [44], with modifications to the Antarctic topography as a result of the asynchronous coupling. The GCM uses the BIOME4 vegetation model, with changes in vegetation used to update the surface type in the RCM. The GCM is oxygen isotope enabled. We first perform a cool climate simulation with atmospheric CO₂ of 280 ppm and a cool austral astronomical configuration (January insolation at 70°S = 465 Wm⁻²). These meteorological boundary conditions (6-hourly saves) are then used by the RCM (RegCM3 [45]), which has a resolution of 80×80 km. The RCM is not isotope enabled so we use the $\delta^{18}\text{O}$ of precipitation from the GCM. A uniform correction (-10 ‰) is applied to the $\delta^{18}\text{O}$ of precipitation because of a heavy bias when compared with modern estimates [46]. The climate output from the RCM (temperature and precipitation) is used to force the ice sheet model. A correction of +2°C is applied to RCM temperatures because of a cool bias in control simulations when compared with modern temperatures. As detailed simulation of sub-ice-shelf warming on these timescales is not currently feasible, sub-surface ocean temperatures are from a high-resolution modern dataset. The ice sheet is allowed to equilibrate with the cold climate forcing, starting from either a modern ice sheet (Scenario A) or ice-free conditions for Scenario B, which takes 150 kyrs.

Next an instantaneous warming experiment is performed. This uses the equilibrated ice sheets from the colder climate simulations as boundary- and initial-conditions. Atmospheric CO₂ is increased to either 500 or 840 ppm and a warm austral summer astronomical configuration is specified (January insolation at 70°S = 539 Wm⁻²). Because of the significant computational expense of the asynchronous GCM-RCM climate forcing it is not currently feasible to perform simulations with a transient astronomical forcing. Following earlier work [23,43], for warmer climate GCM simulations the ocean heat flux in the southern ocean is increased to maintain ice-free conditions following the collapse of the West Antarctic ice sheet. This increased heat flux does not drive ice sheet collapse, and sensitivity tests without the increased heat flux yield similar results (see *Supporting Information*). A uniform sub-surface ocean warming of 2 °C is added to the modern dataset. Coupling between the GCM-RCM-ISM is performed for the first 2 iterations (i.e. 0 kyr and 2 kyr into the simulation), because of large changes in the land-sea mask. For subsequent iterations (every 2 kyr) the ice sheet model is coupled directly to the RCM, with the GCM boundary conditions held constant. We rerun the GCM at the end of the simulation to obtain $\delta^{18}\text{O}$ of precipitation for the final

681
682
683
684
685
686
687
688
689
690
691
692
693
694
695
696
697
698
699
700
701
702
703
704
705
706
707
708
709
710
711
712
713
714
715
716
717
718
719
720
721
722
723
724
725
726
727
728
729
730
731
732
733
734
735
736
737
738
739
740
741
742
743
744
745
746
747
748

ice sheet configuration. The mean oxygen isotopic composition of the ice sheet is converted to a mean seawater oxygen isotope value following [48]. All sea level equivalent values in the manuscript are for ice above floatation, accounting for the infilling with seawater of ocean basins below sea level

- Zachos JC, Dickens GR, Zeebe RE (2008) An early Cenozoic perspective on greenhouse warming and carbon-cycle dynamics. *Nature* 451:279–283
- Holbourn A, Kuhnt W, Clemens S, Prell W, Andersen N (2013) Middle to late Miocene stepwise climate cooling: Evidence from a high-resolution deep water isotope curve spanning 8 million years. *Paleoceanography*, 28:688–699
- Liebrand D, et al. (2011) Antarctic ice sheet and oceanographic response to eccentricity forcing during the early Miocene. *Climate of the Past* 7:869–880
- Shevenell AE, Kennett JP, Lea DW (2008) Middle Miocene ice sheet dynamics, deep-sea temperatures, and carbon cycling: A Southern Ocean perspective. *Geochemistry, Geophysics, Geosystems* 9(2):GC001736
- Lear CH, Mawbey EM, Rosenthal Y (2010) Cenozoic benthic foraminiferal Mg/Ca and Li/Ca records: Toward unlocking temperatures and saturation states. *Paleoceanography* 25:PA4215
- Miller KG, et al. (2005) The Phanerozoic Record of Global Sea-Level Change. *Science* 310(5752):1293–1298
- Kominz MA, et al. (2008) Late Cretaceous to Miocene sea-level estimates from the New Jersey and Delaware coastal plain coreholes: an error analysis. *Basin Research* 20:211–226
- John CM, et al. (2011) Timing and magnitude of Miocene eustasy derived from the mixed siliclastic-carbonate stratigraphic record of the northeastern Australian margin. *Earth and Planetary Science Letters* 304:455–467
- de Boer B, Van de Wal RSW, Bintanja R, Lourens LJ, Tuenter E (2010) Cenozoic global ice-volume and temperature simulations with 1-D ice-sheet models forced by benthic $\delta^{18}\text{O}$ records. *Annals of Glaciology* 51(55):23–33
- Warny S, et al. (2009) Palynomorphs from sediment core reveal a sudden remarkably warm Antarctica during the Mid Miocene. *Geology* 37(10):955–958
- Feakins SJ, Warny S, Lee J-E (2012) Hydrologic cycling over Antarctica during the middle Miocene warming. *Nature Geoscience* 5(8):557–560
- Hauptvogel DW, Passchier S (2012) Early–Middle Miocene (17–14 Ma) Antarctic ice dynamics reconstructed from the heavy mineral provenance in the AND-2A drill core, Ross Sea, Antarctica. *Global and Planetary Change* 82–83:38–50
- Passchier S, et al. (2011) Early and middle Miocene Antarctic glacial history from the sedimentary facies distribution in the AND-2A drill hole, Ross Sea, Antarctica. *GSA Bulletin* 123(11–12):2352–2365
- Lewis AR, et al. (2008) Mid-Miocene cooling and the extinction of tundra in continental Antarctica. *Proc Natl Acad Sci* 105(31):10676–10680
- Kurschner WM, Kvacek Z, Dilcher D (2008) The impact of Miocene atmospheric carbon dioxide fluctuations on climate and the evolution of terrestrial ecosystems. *Proc Natl Acad Sci* 105(2):449–453
- Foster GL, Lear CH, Rae JWB (2012) The evolution of pCO₂, ice volume and climate during the middle Miocene. *Earth and Planetary Science Letters* 341–344:243–254
- Badger MPS, et al. (2013) CO₂ drawdown following the middle Miocene expansion of the Antarctic Ice Sheet. *Paleoceanography*, 28:42–53
- Greenop R, Foster GL, Wilson PA, Lear CH (2014) Middle Miocene climate instability associated with high-amplitude CO₂ variability. *Paleoceanography* 29:845–853
- Zhang YG, Paganí M, Liu Z, Boharty SM, DeConto R (2013) A 40-million-year history of atmospheric CO₂. *Phil Trans R Soc A* 371:20130096
- Pollard D, DeConto R (2005) Hysteresis in Cenozoic Antarctic ice-sheet variations. *Global and Planetary Change* 45:9–21
- Langebroek PM, Paul A, Schulz M (2009) Antarctic ice-sheet response to atmospheric CO₂ and insolation in the Middle Miocene. *Climate of the Past* 5:633–646
- Huybrechts P (1993) Glaciological modeling of the late Cenozoic East Antarctic Ice Sheet: stability or dynamism? *Geogr. Ann* 75A:221–238
- Pollard D, DeConto RM, Alley RB (2015) Potential Antarctic Ice Sheet retreat driven by hydrofracturing and ice cliff failure. *Earth and Planetary Science Letters* 412, 112–121
- Oerlemans J (2002) On glacial inception and orography. *Quaternary International* 95–96:5–10
- Mengel M, Levermann A (2014) Ice plug prevents irreversible discharge from East Antarctica. *Nature Climate Change* 4:451–455
- Cook CP, et al. (2013) Dynamic behavior of the East Antarctic ice sheet during Pliocene warmth. *Nature Geoscience* 6:765–769
- Rovere A, et al. (2014) The Mid-Pliocene sea-level conundrum: Glacial isostasy, eustasy and dynamic topography. *Earth and Planetary Science Letters* 387:27–33
- Miller KG, et al. (2012) High tide of the warm Pliocene: Implications of global sea level for Antarctic deglaciation. *Geology* G32869.1
- Weertman J (1974) Stability of the junction between an ice sheet and an ice shelf. *Journal of Glaciology* 13(67):3–11
- Schoof C (2007) Ice sheet grounding line dynamics: Steady states, stability, and hysteresis. *Journal of Geophysical Research* 112(F3):F03S28
- Fretwell P, et al. (2013), Bedmap2: improved ice bed, surface and thickness datasets for Antarctica. *The Cryosphere* 7(1):375–393
- Golledge NR, Fogwill CJ, Mackintosh AN, Buckley KM (2012) Dynamics of the last glacial maximum Antarctic ice-sheet and its response to ocean forcing. *Proc Natl Acad Sci* 109(40):16052–16056
- DeConto RM, et al. (2008) Thresholds for Cenozoic bipolar glaciation. *Nature* 455:652–656
- Wilson DS, et al. (2012) Antarctic topography at the Eocene–Oligocene boundary. *Paleoceanography, Palaeoclimatology, Palaeoecology* 335–336:24–34
- Lewis AR, Marchant DR, Ashworth AC, Hemming SR, Machlus ML (2007) Major middle

once ice has retreated; these values should be used for comparison with eustatic sea level records. These values are not used for calculations of $\delta^{18}\text{O}_{\text{sw}}$, because this infilling effect is not relevant to the total ice volume recorded by $\delta^{18}\text{O}_{\text{sw}}$ (i.e. ice both above and below floatation).

- Miocene global climate change: Evidence from East Antarctica and the Transantarctic Mountain. *GSA Bulletin* 119(11–12):1449–1461
- Retallack GJ (2009) Refining a pedogenic-carbonate CO₂ paleobarometer to quantify a middle Miocene greenhouse spike. *Paleoceanography, Palaeoclimatology, Palaeoecology* 281:57–65
- Unger N, Yue X (2014) Strong chemistry-climate feedbacks in the Pliocene. *Geophysical Research Letters* 41:527–533
- Goldner A, Herold N, Huber M (2014) The challenge of simulating the warmth of the mid-Miocene climatic optimum in CESM1. *Climate of the Past* 10:523–536
- Weertman J (1974) Stability of the junction between an ice sheet and an ice shelf. *Journal of Glaciology* 13(67):3–11
- Pollard D, DeConto RM (2012) Description of a hybrid ice sheet-shelf model, and application to Antarctica. *Geoscientific Model Development* 5(5):1273–1295
- Jamieson SR, et al. (2014) The glacial geomorphology of the Antarctic ice sheet bed. *Antarctic Science* 26(6):724–741
- Thompon S, Pollard D (1997) Greenland and Antarctic mass balances for present and doubled atmospheric CO₂ from the GENESIS Version-2 Global Climate Model. *Journal of Climate* 10:871–900
- DeConto RM, Pollard D, Kowalewski D (2012) Modeling Antarctic ice sheet and climate variations during Marine Isotope Stage 31. *Global and Planetary Change* 88–89:45–52
- Herold N, Seton M, Müller RD, You Y, Huber M (2008) Middle Miocene tectonic boundary conditions for use in climate models. *Geochemistry, Geophysics, Geosystems* 9(10):Q10009
- Pal J, et al. (2007) Regional climate modelling for the developing world: the ICTP RegCM3 and RegCM3. *Bull. Am. Meteor. Soc.* 88:1395–1409
- Mathieu R, et al. (2002) Simulation of stable water isotope variations by the GENESIS GCM for modern conditions. *J. Geophys. Res.* 107(D4):4037
- Mudelsee M, Bickert T, Lear CH, Lohmann G (2014) Cenozoic climate changes: a review based on time series analysis of marine benthic $\delta^{18}\text{O}$ records. *Rev. Geophysics* 52: 2013RG000440
- Langebroek PM, Paul A, Schulz M (2010) Simulating the sea level imprint on marine oxygen isotope records during the middle Miocene using an ice sheet-climate model. *Paleoceanography* 25(4):PA4203
- Gasson E, DeConto R, Pollard D (2015) Antarctic bedrock topography uncertainty and ice sheet stability. *Geophysical Research Letters* doi:10.1002/2015GL064322
- Pollard D (2010) A retrospective look at coupled ice sheet-climate modeling. *Climatic Change* 100:173–194
- Chow JM, Bart PJ (2003) West Antarctic Ice Sheet grounding events on the Ross Sea outer continental shelf during the middle Miocene. *Paleoceanography, Palaeoclimatology, Palaeoecology* 198:169–186
- Gasson E, et al. (2014) Uncertainties in the modelled CO₂ threshold for Antarctic glaciation. *Climate of the Past* 10:451–466
- DeConto R, Pollard D (2003) Rapid Cenozoic glaciation of Antarctica induced by declining atmospheric CO₂. *Nature* 421:245–249
- Huybrechts P, et al. (2011) Response of the Greenland and Antarctic ice sheets to multi-millennial greenhouse warming in the Earth system model of intermediate complexity LOVECLIM. *Surv. Geophys.* 32:397–416
- Bassis JN, Walker CC (2011) Upper and lower limits on the stability of calving glaciers from the yield strength envelope of ice. *Proc. R. Soc. A* doi:10.1098/rspa.2011.0422
- DeConto R, Pollard D, Harwood D (2007) Sea ice feedback and Cenozoic evolution of Antarctic climate and ice sheets. *Paleoceanography* 22:PA3214
- Haywood A, et al. (2011) Are there pre-Quaternary geological analogues for a future greenhouse warming? *Phil. Trans. R. Soc. A* 369:933–956
- Wilson DS, Pollard D, DeConto R, Jamieson S, Luyendyk BP (2013) Initiation of the West Antarctic Ice Sheet and estimates of total Antarctic ice volume in the earliest Oligocene. *Geophysical Research Letters* 40:4305–4309
- Gasson E (2013) The past relationship between temperature and sea level – from proxy records and ice sheet modeling. *PhD Thesis*, University of Bristol, UK
- Winnick MJ, Cave JK (2015) Oxygen isotope mass-balance constraints on Pliocene sea level and East Antarctic Ice Sheet stability. *Geology* 43:879–882
- Austermann J, et al. (2015) The impact of dynamic topography change on Antarctic ice sheet stability during the mid-Pliocene warm period. *Geology* 43:927–930
- Holbourn A, Kuhnt W, Schulz M, Flores J-A, Andersen N (2007) Orbitally-paced climate evolution during the middle Miocene “Monterey” carbon-isotope excursion. *Earth and Planetary Science Letters* 261:534–550
- Foster GL, Rohling EJ (2013) Relationship between sea level and climate forcing by CO₂ on geological timescales. *PNAS* 110(4):1209–1214
- Jamieson SR, Sugden DE, Hulton, NR (2010) The evolution of the subglacial landscape of Antarctica. *EPSL*
- Hambrey MJ, McKelvey B (2000) Major Neogene fluctuations of the East Antarctic ice sheet: stratigraphic evidence from the Lambert Glacier region. *Geology* 28(10):887–890
- Williams T, Handwerger D (2005) A high-resolution record of early Miocene Antarctic glacial history from ODP site 1165, Prydz Bay. *Paleoceanography* 20:PA2017
- Fyke JG, et al. (2011) A new coupled ice sheet/climate model: description and sensitivity to model physics under Eemian, Last Glacial Maximum, late Holocene and modern climate conditions. *Geosci. Model Dev.* 4:117–136

749
750
751
752
753
754
755
756
757
758
759
760
761
762
763
764
765
766
767
768
769
770
771
772
773
774
775
776
777
778
779
780
781
782
783
784
785
786
787
788
789
790
791
792
793
794
795
796
797
798
799
800
801
802
803
804
805
806
807
808
809
810
811
812
813
814
815
816